Spherical optical model potential for the Re/Os stellar nucleosynthesis chronometer from s-wave neutrons on ^{186,187,188}Os

R. R. Winters
Department of Physics, Denison University, Granville, Ohio 43023

R. F. Carlton
Department of Chemistry and Physics, Middle Tennessee State University, Murfreesboro, Tennessee 37132

J. A. Harvey and N. W. Hill
Oak Ridge National Laboratory, Oak Ridge, Tennessee 37831
(Received 3 February 1986)

This paper reports resonance parameters and spherical optical model potentials obtained from the analyses of neutron transmission measurements for ^{186,188}Os over the incident neutron energy range 27–1000 eV and for ^{187}Os over the range 27–140 eV. Multilevel R-matrix analyses of 77 s-wave resonances yielded sets of resonance parameters (E_λ, Γ_n) and the associated external (background) R functions. The statistical properties of the resonance parameters, mean-level spacings, and strength functions are reported. The external R functions and strength functions were used to determine spherical optical model potential well depths, which in the case of ^{187}Os we find to be strongly dependent on the spin of the compound nucleus. These optical model well depths can be used to estimate the capture cross section of the first excited state in ^{187}Os+n. Since this state is highly populated at stellar temperatures, the ratio of excited to ground-state capture cross sections is an important parameter in using the s-process model of stellar nucleosynthesis to determine what fraction of the abundance of ^{187}Os should be ascribed to the radiogenic decay of ^{187}Re. That fraction determines, in part, the estimate of the duration Δ of stellar nucleosynthesis to be derived from ^{187}Re beta decay. A determination of Δ for the Re/Os chronometer based on our data leads to an age of the universe of $(17\pm3)\times10^9$ yr.

I. INTRODUCTION

Attempts to estimate the duration and evolution of stellar nucleosynthesis have been among the most exciting activities in astrophysics since the idea was first suggested by Alpher and Herman[1] and Burbridge *et al.*[2] nearly 35 years ago. That the decay of long-lived radioactive nuclides produced in the stars should carry the signature of nucleosynthetic processes was first recognized and exploited by Fowler and Hoyle[3] to estimate the duration of nucleosynthesis via U/Th radioactive decay. Subsequently, other long-lived radioactive progenitors subsequently have been identified[4] as potential nucleosynthesis chronometers. Of these, the one most prominently featured in the literature has been ^{187}Re, which beta decays to ^{187}Os with a half-life of $\sim4\times10^{10}$ yr, a time comparable to the Hubble time. This long half-life and the fact that both ^{186}Os and ^{188}Os can be produced only by s-process nucleosynthesis make this chronometer potentially the most reliable available. That a completely satisfactory realization of Re/Os as a reliable chronometer has not yet been achieved is evident in the literature surrounding the question of stellar temperature and pressure effects on ^{187}Re decay,[5–11] the chemical evolution[11] of galactic material, and the relative importance of neutron capture by the low-lying first excited state in ^{187}Os.[4]

The particularly thorough review of Arnould *et al.*[12] emphasizes that an important contribution to the uncertainty associated with the use of Re/Os as a chronometer remains the estimation of the modification of the ratio of average neutron-capture cross sections $\langle\sigma_\gamma(186)\rangle/\langle\sigma_\gamma(187)\rangle$ due to population of the 9.75-keV first excited state in ^{187}Os at stellar temperatures. This stellar enhancement factor f^* was first calculated by Woosley and Fowler[13] using a Hauser-Feshbach model for the cross sections for both the ground and the excited states. The transmission factors for the Hauser-Feshbach calculation were estimated from the few exiting measurements in the mass region near osmium.

In this paper we present additional neutron transmission measurements for ^{186,188}Os over the incident neutron energy range from 27 to 1000 eV and for ^{187}Os over the range from 27 to 140 eV, together with the statistical properties of the neutron-resonance parameters and the optical model potential well depths obtained from the data. Preliminary values of our results were used by Herschberger *et al.*[14] to recalculate f^*, and their value of $f^*=0.81\pm0.02$ is in good agreement with the earlier Woosley-Fowler estimate of $0.75\le f^*\le1.2$. These results, coupled with recent measurements[14,15] of the ^{187}Os(n,n′) and ^{189}Os(n,γ) cross sections, seem to suggest that f^* can now be calculated with an uncertainty of less than 5%, i.e., with an uncertainty comparable to those of the cross-section measurements.

II. TRANSMISSION MEASUREMENTS

The neutron transmissions of ^{186,187,188}Os (see Fig. 1 for a representative energy region) were measured using the time-of-flight technique at the Oak Ridge Electron Linear Accelerator (ORELA). The accelerator was pulsed at 800 bursts/s with a nominal electron burst width of 33 ns. The resulting neutron burst has a continuous spectrum produced by the photoneutron process in tantalum with subsequent moderation in the 15-cm-diam beryllium-clad water-filled target housing. The target is 3.2 cm thick in the direction of the neutron flight path. Neutrons were detected via the ^{6}Li(n,α) reaction in a 1.3-cm-thick and 11-cm-diam ^{6}Li glass scintillator mounted on a 12.7-cm photomultiplier tube. The flight-path length from target to detector was 79.46±0.02 m, where the uncertainty estimate includes uncertainties in the moderator and detector effective thicknesses. The arrival time of each detected neutron was measured with a digital time analyzer to within 0.01% of its flight time relative to the arrival of the gamma-ray burst originating in the neutron-producing target. All counts were corrected for the 1104-ns dead time of the analyzer. This correction was less than 0.1% below 1000 eV.

The neutron-energy resolution function at energy E is expected to be a combination in quadrature of the fluctuations in flight-path length and apparent flight time and has been found[16] to have an approximately Gaussian shape with a full width at half maximum ΔE given by

$$(\Delta E/E)^2=(a+bE)\times 10^{-6}\ ,$$

where $a=0.23$ and $b=50\ \mathrm{MeV}^{-1}$.

Four components of background have been identified: (a) a time-independent room background, (b) 2.23-MeV gamma rays which are due to neutron capture by hydrogen in the target/moderator and which decay with a 17-μs half-life, (c) neutrons scattered from the detector and environment, and (d) delayed pulses within the phototube associated with the gamma burst. The last background was reduced by placing a 6 mm lead filter in the neutron beam

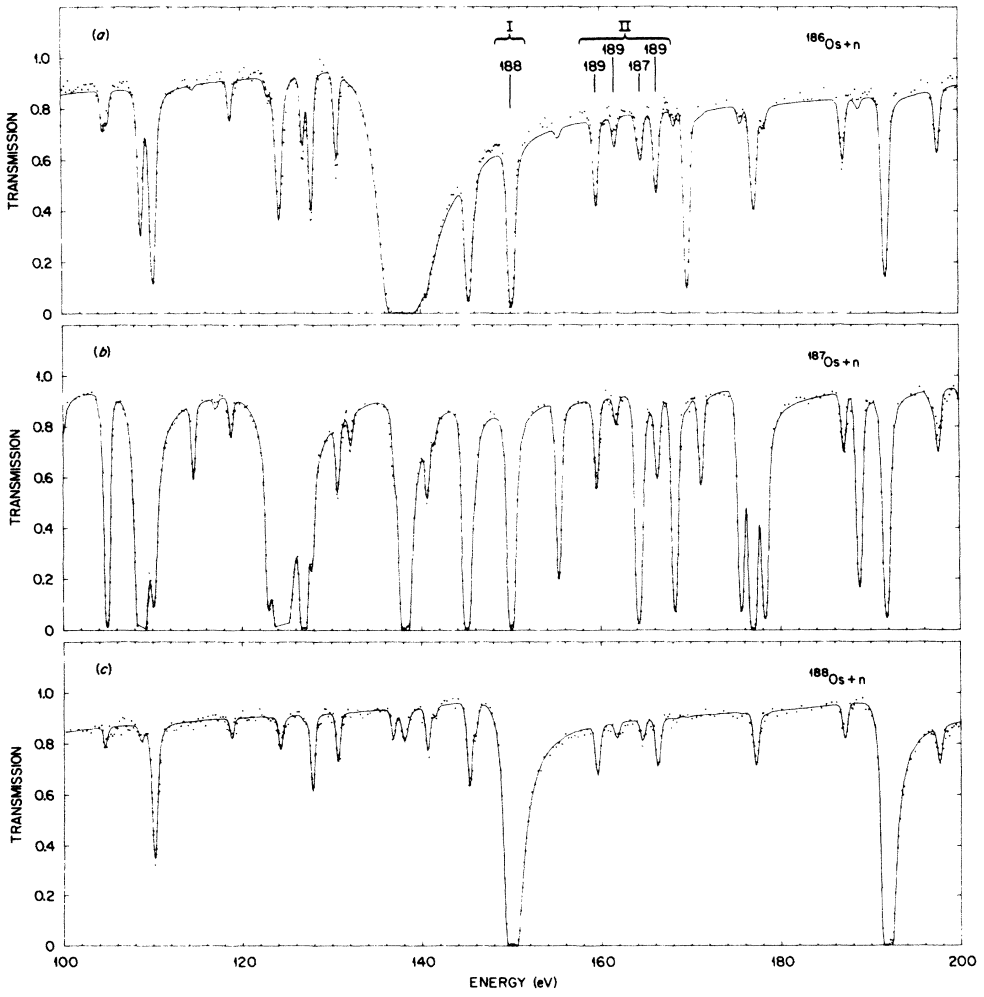

FIG. 1. Neutron transmissions for the three samples with major concentrations of (a) ^{186}Os, (b) ^{187}Os, and (c) ^{188}Os over the energy range 100–200 eV. The region labeled I includes the 150-eV resonance in ^{188}Os as observed in all three samples. The region labeled II includes three impurity resonances due to ^{189}Os. The curve is the result of solving Bayes's equations for the optimal set of resonance parameters to describe these data.

TABLE I. Representative factors applied to observed counts to correct for (a) time-independent room background, (b) 2.23 MeV gamma rays from H(n,γ), and (c) neutrons scattered from the detector and environment. [(a)–(c) are in percent.]

E_n (keV)	(a)	(b)	(c)
60	0.4	2	2.5
7	0.7	0.3	2.5
1	1.5	~0	2.0
0.07	9.2	~0	2.0

and by gating the detector on only after the gamma burst. In order to reduce the number of very slow neutrons overlapping with the succeeding bursts, a ^{10}B filter was also placed in the neutron beam. With this arrangement, the background components are very small (see Table I). A more complete discussion of the experimental details of ORELA transmission measurements has been given by Larson *et al.*[16]

The isotopically enriched osmium samples were sintered metal hot-pressed into 1-cm-diam cylinders ~2 mm thick. The thicknesses and isotopic compositions of the osmium samples are given in Table II. The samples were cycled into and out of the neutron beam under computer control with a cycle time of approximately 10 min per sample. A 10-min run per cycle was also made with no sample in the beam. In addition, four positions in the sample holder were loaded with pieces of polyethylene 2.54 cm thick to allow a determination of the 2.23-MeV gamma-ray background mentioned earlier.

III. DATA ANALYSIS

A. The *R*-matrix formalism

The total cross section for the case of a neutron with wave number k incident on a target forming states with total and orbital angular momentum quantum numbers J,l can be written

$$\sigma_{nT}=\frac{2\pi}{k^2}\sum_{J,l} g(J)[1-\mathrm{Re}(U^{Jl}_{nn})] . \tag{1}$$

In the R-matrix formalism, the scattering function U^{Jl}_{nn} is expressible, for the single-channel case, as

$$U^{Jl}_{nn}(E)=e^{2i\phi_l}\left[\frac{1-R^J_l(S_l-B_l-iP_l)}{1-R^J_l(S_l-B_l+iP_l)}\right] . \tag{2}$$

In this expression, ϕ_l, S_l, B_l, and P_l are the hard sphere phase shifts, shift factors, boundary conditions, and neutron penetrabilites, respectively, and are to be evaluated at the channel radius, chosen in this work as $a_c=7.70$ fm. The boundary conditions were chosen as $B_l=-l$.

The R^J_l constitutes the R matrix, which for a given channel (Jl) is expressed in terms of the levels observed in the region of analysis and an external R function,

$$R^J_l(E)=\sum_\lambda \frac{\gamma^2_{n\lambda}}{E_\lambda-E-i\Gamma_{\gamma\lambda}/2}+R^{ext}_{Jl}(E) . \tag{3}$$

Here, $\gamma_{n\lambda}$, $\Gamma_{\gamma\lambda}$, and E_λ are the reduced neutron-width amplitude, the radiation width, and the eigenenergy for the λth resonance. The sum is taken over all levels of the given Jl observed in the energy region $[E_L,E_u]$ of the measurement. The $\gamma^2_{n\lambda}$'s are related to the neutron widths Γ_n by the relation

$$\gamma^2_{n\lambda}=\Gamma_{n\lambda}/2P_l . \tag{4}$$

The functions R^{ext}_{Jl} describe the tails of resonances located external to the region $[E_L,E_u]$. The functional form for the background functions,

$$R^{ext}_{Jl}(E)=\tilde{R}_{Jl}(E)-\tilde{s}_{Jl}\ln\left[\frac{E_u-E}{E-E_L}\right] , \tag{5}$$

used in this analysis is thoroughly discussed in Refs. 17–19. The logarithmic term in Eq. (5) represents a continuous distribution of neutron strength $\tilde{s}_{Jl}$ below and above $[E_L,E_u]$. In this work $\tilde{s}_{Jl}$ is taken to be the strength function observed in $[E_L,E_u]$,

$$\tilde{s}_{Jl}=\langle\gamma^2_{nJl}\rangle/\langle D_{Jl}\rangle . \tag{6}$$

Since $\tilde{R}_{Jl}(E)$ is a mild function of energy (see Ref. 17), it is sufficient to represent $\tilde{R}_{Jl}$ with a linear form,

$$\tilde{R}_{Jl}(E)=\alpha_{Jl}+\beta_{Jl}E . \tag{7}$$

This representation of R^{ext}_{Jl} provides a very accurate description[19] of the interference between the observed levels and backgrounds. In turn, an accurate determination of R^{ext} provides considerable information about the aggregate effect at a given energy E, $E_L<E<E_u$, of all resonances external to the analysis region, and represents an important measure of the *average* properties of all levels of each channel (Jl). At low energy the s-wave background R function is related to the potential scattering

TABLE II. Isotopic composition (in at. %) of the osmium samples. Elemental impurities are <1.8% for the ^{186}Os sample, <1.2% for the ^{187}Os sample, and <0.04% for the ^{188}Os sample.

Enriched isotope	184	186	187	188	189	190	192
186[a]	<0.02	79.39(15)[b]	1.62(3)	5.07(5)	4.09(4)	5.15(5)	5.67(6)
187[a]	<0.05	0.93(2)	70.38(15)	12.79(10)	5.28(5)	5.41(5)	5.26(5)
188[a]	<0.05	0.13(3)	0.17(3)	94.47(20)	2.77(5)	1.42(4)	1.04(4)

[a]Sample thicknesses (in nuclei of osmium/b): $n(186)=0.012\,75$, $n(187)=0.008\,401$, and $n(188)=0.008\,221$.

[b]Uncertainty estimates in this and all following tables are in parentheses and are to be interpreted as uncertainty in the last digits as quoted, e.g., 78.39±0.15.

length R'_{Jl} by

$$R'=a_c[1-\tilde{R}(E)]\ , \tag{8}$$

where $\tilde{R}$ is evaluated for $E\rightarrow 0$. In the past $\tilde{R}$ has been referred[20] to as R^{∞}, the distant level parameter. The $\tilde{R}$ obtained from the fitting process is dependent on the choice for a_c, but the calculated value for R' is independent of a_c. In the spin-separated case of ^{187}Os (discussed below), different R' values are found to be necessary to fit the $J=0$ and 1 resonances.

The parameters E_λ, $\gamma^2_{n\lambda}$, and R^{ext}_{Jl} which produced the best description of the observed transmissions were determined by solving Bayes's equations[21] using the R-matrix code MULTI.[22] The fitting procedure included Doppler broadening of the calculated cross sections and resolution broadening to the resulting transmissions. Throughout the analysis, the small ($\sim$0.08-eV) radiative widths have been held constant and equal to the average values reported in Table II of Winters and Macklin.[23] All resonances up to 1000 eV are assumed to be s wave. In many cases the characteristic asymmetry in the transmission gives visual confirmation of that assumption. For resonances so narrow as to be resolution dominated, the assignment of $l=0$ is supported by the small likelihood of a resonance with $l>0$ having a width sufficiently large to be observed for $E<1000$ eV.

While the significant abundances of isotopic impurities in each sample presented difficulties, the fact that each resonance appears in each of the three osmium samples allowed improvement of the precision of our estimates of the resonance parameters by providing three sample thicknesses. The three sample thicknesses for each resonance also allowed confirmation of isotopic parentage in the case of the ^{186,187,188}Os resonances. In order to avoid spurious isotopic level assignments, we imposed two requirements on the fitting procedure: (a) parameters for large isolated resonances (see, e.g., the region labeled I in Fig. 1) deduced in the sample of largest isotopic abundance had to also adequately describe that resonance treated as an impurity in the other two samples, and (b) other isotopic ($A=189,190,192$) impurity contributions (see, e.g., the region labeled II in Fig. 1) had to be reasonably well reproduced in all three samples by identical parameters. Using these criteria we were also able to reduce the uncertainties for parameters in cases where the impurity resonance overlapped with that of the major isotope. The resulting sample-consistent, single-parameter set will therefore reproduce all three observed transmission spectra. Multilevel fits to the transmissions in a typical energy region are shown as the solid smooth curves in Fig. 1. The resulting R-matrix level parameters over the range 27–1000 eV for ^{186}OS and ^{188}Os and over the range 27–140 eV for ^{287}Os are presented in Tables III–V. For energies greater than these upper limits, only the most prominent s-wave resonances for each isotope were analyzed. These level parameters and all R-matrix parameters obtained in this work for ^{186,187,188}Os up to 3400, 1000, and 5000 eV, respectively, have been transmitted to the National Nuclear Data Center in Brookhaven.

IV. RESONANCE PARAMETER STATISTICS

The statistical properties of the R-matrix resonance parameters of most importance are the strength function, the average level spacings, and the external R functions. In the electron-volt energy region, the s-wave R-matrix reduced widths and strength function are proportional to the more commonly reported[20] s-wave conventional reduced widths Γ^0_n and strength function S_0,

$$\Gamma^0_n=2ba_c\gamma^2_{nJl} \tag{9}$$

TABLE III. Resonance parameters for ^{186}Os + n up to 1 keV neutron energy.

E_n (eV)[a]	Γ_n (meV)[b]	l	E_n (eV)[a]	Γ_n (meV)[b]	l
44.7	85.0(4)[c]	0	521.0	149(2)	0
66.3	28.9(3)[c]	0	567.8	243(3)	0
89.7	11.5(3)	0	604.6	51(2)	0
137.7	429(6)	0	634.7	198(6)	0
169.7	5.7(2)	0	643.5	509(7)	0
201.9	61.9(6)	0	655.3	462(6)	0
249.5	17.0(3)	0	679.7	342(6)	0
272.9	1.9(1)	(0)[d]	735.8	11(1)	(0)[d]
281.0	142(2)	0	763.0	123(2)	0
313.4	41.2(6)	0	796.8	57(2)	0
342.4	668(6)	0	837.1	362(6)	0
370.0	156(3)	0	845.8	42(2)	0
380.0	138(4)	0	868.5	724(8)	0
416.8	42.2(5)	0	891.3	103(4)	0
423.1	123(6)	0	962.6	1610(150)	0
452.1	17.0(5)	0	980.0	819(50)	0

[a]Energy uncertainties may be taken as one resolution width as discussed in text.
[b]Radiation widths have been assumed constant at 80 meV based on averages obtained in Ref. 23.
[c]The notation 28.9(4) means 28.9±0.4. The quoted uncertainties are those due to counting statistics and the fitting procedure and do not include an overall systematic uncertainty of $\sim$2%.
[d]Parentheses indicate uncertainty in the l assignment.

TABLE IV. Resonance parameters for ^{187}Os + n from 26 to 140 eV neutron energy.

E_n (eV)[a]	$g\Gamma_n$ (meV)[b]	J	E_n (eV)[a]	$g\Gamma_n$ (meV)[b]	J
29.33	0.51(4)[c]	1	92.84	10.4(2)	1
39.51	2.28(7)	1	99.24	60.1(3)	0
40.54	12.4(5)	1	104.96	13.9(3)	1
43.48	10.9(6)	1	108.79	123.4(12)	1
47.80	15.9(5)	1	110.96	0.54(3)	(0)[f,g]
50.06	52.7(8)	0	114.59	1.43(8)	(1)
50.59	7.0(9)	1	117.11	0.53(3)	(0)[f]
62.16	18.2(11)	0[e]	122.94	6.21(3)	1
63.76	70.9(3)	0	124.33	498.2(12)	0
65.01	1.65(7)	1	126.89	47.1(12)	1
71.43	1.09(5)	1	132.13	0.68(10)	(1)[f]
83.36[d]	0.71(5)	1	138.13	109.3(22)	1[f]
89.90	19.1(9)	1			

[a]Energy uncertainties may be taken as one resolution width as discussed in the text.
[b]Radiation widths have been assumed constant at 78 meV based on averages obtained in Ref. 23.
[c]In this notation $0.51(4) \equiv 0.51 \pm 0.04$. See footnote c in Table III.
[d]Stolvy *et al.* (Ref. 25) reports a $J=0$ resonance at 78 eV and a $J=1$ resonance at 79.5 eV.
[e]The assignment $J=1$ is made in Ref. 25.
[f]No J assignment given in Ref. 25.
[g]Parentheses indicate that the J assignment is uncertain.

and

$$S_0 = \langle \Gamma_n^0 \rangle / \langle D \rangle = 2ba_c\tilde{s} , \tag{10}$$

where D is the level spacing for a given J and

$$b \equiv (0.219\,68 \times 10^{-3}) A (A + 1.0089)^{-1} .$$

The relationship between the Γ_n^0 and γ_n^2 and between S_0 and $\tilde{s}$ are discussed in Refs. 17 and 18.

In estimating $\langle \gamma_n^2 \rangle$ and $\langle D \rangle$ from the sets of resonance parameters for each isotope and spin, corrections were made for missed levels and their associated strength. These corrections are based on the probability of drawing a width smaller than the smallest observed reduced width from a Porter-Thomas (PT) distribution with mean reduced width equal to that observed. As an additional aid in detecting both missed and spuriously assigned levels, the Dyson-Mehta Δ_3 statistic was calculated for each parameter set, including singly and in all combinations of all levels with doubtful assignments. An additional concern is the identification of p-wave resonances as small s waves. Assuming a p-wave strength function and level spacing typical of the mass region near osmium, we estimate the probability that a p-wave resonance will have an observed width as large as the smallest s-wave below 1000 eV to be less than 0.10%. Hence, we expect to see no p-wave resonances below 1000 eV. In the following we present, by isotope, special problems encountered in fitting the transmissions and the results of the analyses.

A. ^{186}Os

Over the energy range 27—1000 eV we observed 32 resonances in ^{186}Os + n. A previous study[20,24] reported 31 resonances below 1000 eV. The present work confirms all but one previous isotopic assignment (at 721 eV), which we attribute to ^{192}Os. Furthermore, our sample-consistent impurity analysis allows the isotopic identification as ^{186}Os for two additional levels, at 272 and 342 eV. Finally, one additional resonance, at 345 eV, was considered for assignment to ^{186}Os but was rejected by the Δ_3 test.

TABLE V. Resonance parameters for ^{188}Os + n up to 1 keV neutron energy.

E_n (eV)[a]	Γ_n (meV)[b]	l	E_n (eV)[a]	Γ_n (meV)[b]	l
38.73	42(5)[c]	0	536.5	85(2)	0
78.5	378(3)	0	620.1	108(3)	0
150.0	144(1)	0	649.2	70(3)	0
191.9	109(2)	0	705.5	113(5)	0
254.1	73(1)	0	745.2	300(8)	0
282.3	13(1)	0	781.0	1150(30)	0
316.7	957(26)	0	819.5	40(1)	0
388.2	800(26)	0	844.2	1992(60)	0
478.6	486(21)	0	862.6	406(15)	0
528.5	73(1)	0	979.5	133(10)	0

[a]Energy uncertainties may be taken as one resolution width, as discussed in the text.
[b]Radiation widths have been assumed constant at 69 meV based on averages obtained in Ref. 23.
[c]In this notation $42(5) \equiv 42 \pm 5$. See footnote c in Table III.

A cumulative histogram plot of the number of levels is presented in Fig. 2. The linear nature of the plot suggests few missed levels. Adopting a mean reduced s-wave neutron width equal to that observed, we estimate a less than 3% probability that a reduced width drawn from a PT distribution will be smaller than the smallest s wave observed below 1000 eV; i.e., we estimate one missed level. In Fig. 3 is shown a plot of the number of levels exceeding a given reduced width versus the square root of the reduced width. Also shown in the figure are curves calculated from a PT distribution assuming zero and two missed levels. This analysis suggests less than two missed levels. Accordingly, the ^{186}Os mean-level spacing presented in Table VI includes a correction for one missed level. The number of levels, N, in Table VI is the number actually observed.

The external R function for ^{186}Os is shown in Fig. 4 and the parameters for $\tilde{R}$ are given in Table VI. The value of the s-wave scattering length $R'=11.2\pm0.5$ fm is in good agreement with other measurements[20] in this mass region. The strength function (Table VI) $S_0=(3.5\pm0.9)\times10^{-4}$ is consistent with data shown in Fig. 3 of Ref. 20 and helps define the peak in the s-wave strength function due to the $4s_{1/2}$ size resonance.

B. ^{187}Os

We observed a total of 25 resonances in ^{187}Os + n over the energy range 27–140 eV. The two spin states which can be formed as a result of s-wave neutrons incident on a spin-$\frac{1}{2}$ target make the analysis of the data more difficult than for the case of even targets. For that reason we have restricted the following discussion to below 140 eV where J assignments are reported by Stolovy *et al.*[25] The deduced spin values for 27 resonances between 9 and 130 eV on the basis of ratios of gamma-ray intensities associated with neutron capture in the resonances. These assignments and additional ones made in the present work on the basis of level-level interference considerations in the process of fitting have made possible the determination of spin-separated R-matrix resonance parameters for the 25 resonances with neutron energies in the range 27–140 eV shown in Table IV. The mean level spacings

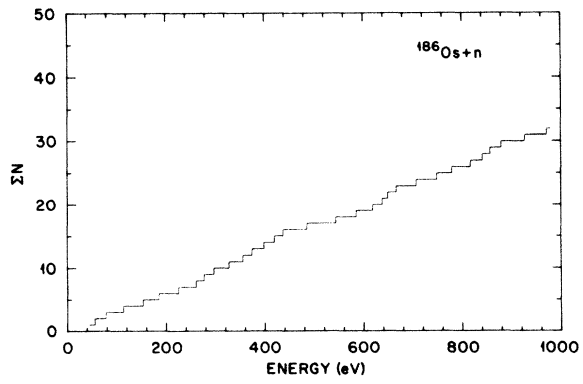

FIG. 2. The cumulative number of levels observed in ^{186}Os + n vs neutron energy. The linear nature of the plot suggests few missed levels.

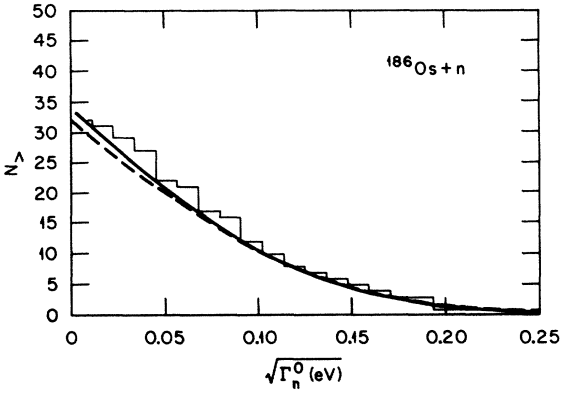

FIG. 3. The number of levels in ^{186}Os + n with $(\Gamma_n^0)^{1/2}$ greater than the abscissa. The dashed and solid curves are the expected results if the widths are drawn from Porter-Thomas distributions with mean widths corresponding to zero and two missed levels, respectively.

$\langle D(0^-)\rangle=10.8\pm2.1$ eV and $\langle D(1^-)\rangle=6.4\pm0.8$ eV are not consistent with a $2J+1$ dependence. This is not surprising since the expected[26] transition in nuclear shape and stability in this mass should modify the dependence on J. Tests (PT and Δ_3) used to estimate the number of missed resonances (Sec. IV A) indicate one missed resonance for the 0^- states and no missed levels for the 1^- states. The Δ_3 statistic is consistent with one missed 0^- level missing below 55 eV where the first 0^- level is observed. The s-wave mean level spacing (corrected for one missed resonance) is 4.0 ± 0.6 eV.

The external R functions for $J=0$ and 1 derived from the multilevel fits below 140 eV differ significantly (see the parameters for $\tilde{R}$ in Table VI). This will be discussed in the next section on the optical model analysis. The scattering lengths, R', are 12.2 ± 1.2 fm for the 0^- levels and 8.9 ± 0.5 fm for the 1^- levels, and are therefore significantly different. A similar result has been reported by Firk *et al.*[27] for ^{51}V. Since, in an optical model, R' is primarily determined by the real well depth, we expect the well depth to be J dependent for ^{187}Os. The calculation of the potential scattering length without regard to the J value requires a spin weighting of the effective cross sections due to each spin group such that

$$\bar{R}'^2=0.25R'^2(J=0)+0.75R'^2(J=1)$$

and (11)

$$\bar{R}'=9.8\pm1.2 \text{ fm} .$$

This result agrees favorably with that based on coupled channel calculations[28] and with values obtained for the other isotopes. The resonance parameter average properties and spin-separated R-matrix parameters for this isotope are presented in Table VI.

C. ^{188}Os

In the range 27–1000 eV, we observed 20 resonances in ^{188}Os + n. Previous work[24] reported 24 resonances below 1000 eV. We attribute two (at 110 and 218 eV) to ^{189}Os and did not observe the resonances reported at 847 and

TABLE VI. Summary of average neutron resonance parameters for osmium isotopes.

A	J	N^a	$\langle D\rangle^b$ (eV)	$\langle\Gamma_n^0\rangle^c$ (meV)	$\langle\gamma^2\rangle$ (meV)	S_0 ($\times 10^4$)	$\tilde{s}$	$\tilde{R}^d$ α	β (keV^{-1})	R'^e (fm)
186	0	32	29.3(27)[f]	10.2(33)	3.0(10)	3.5(9)	0.10(3)	−0.46(6)	0.54(4)	11.2(5)
187	0	7	10.8(21)	8.7(73)	2.6(22)	8.0(45)	0.24(14)	−0.58(15)	−0.81(40)	12.2(12)
187	1	18	6.4(8)	2.1(10)	0.23(31)	3.2(11)	0.096(34)	−0.16(7)	1.01(50)	8.9(5)
188	0	20	47.1(55)	16.9(74)	5.0(20)	3.6(12)	0.11(4)	−0.11(6)	−0.03(2)	8.5(5)

[a]Actual number of levels observed.
[b]Average parameters for $A=186$, 187 ($J=0$), 187 ($J=1$), and 188 are based on corrections for 1, 1, 0, and missing levels, respectively.
[c]The conventional reduced width Γ_n^0 and strength S_0 are discussed in Sec. IV.
[d]$\tilde{R}$ derived from multilevel fits using $a_c=7.7$ fm for the energy interval 0—140 eV for the odd isotope and 0—1000 eV for the even isotopes.
[e]Calculated from Eq. (8) in the text for $a_c=7.7$ fm.
[f]In our notation, 29.3(27)≡29.3±2.7, etc.

896 eV. The Δ_3 statistic (0.33) calculated for the 20 remaining resonances is consistent with the value expected (0.33±0.10) for no spurious or missing levels. Possible spurious levels at 110 and 218 eV (reported earlier) were considered and found to give rise to values of the Δ_3 statistic consistent with that expected. Nonetheless, these resonances appear to be due to ^{189}Os on the basis of the excellent fit obtained for resonances at these energies in all three samples with a single parameter set and assuming them to be due to an impurity. We estimate a 4% probability of observing a resonance smaller than our estimated experimental detection limit for a PT distribution with the observed average reduced width. We have therefore corrected the s-wave mean-level spacing presented in Table VI for one missing level. The strength function $S_0=(3.6\pm1.2)\times10^{-4}$ and $R'=8.5\pm0.5$ fm are similar to the results obtained for ^{186}Os. Individual resonance parameters are presented in Table V.

V. THE SPHERICAL OPTICAL MODEL POTENTIALS

An important application of the phenomenological optical model potential (OMP) has been to describe nuclear scattering for low-energy (< 1000-eV) s-wave neutrons. Over the past two decades the systematics of the OMP well depths over a broad mass region has evolved. This information has proven especially important in developing an understanding of stellar nucleosynthesis since many of the cross sections required in the calculation of chemical abundances either cannot be or have not yet been measured. In the case of the Re/Os chronometer, the capture cross section for the first excited state in ^{187}Os is an example of a cross section unlikely to be measured. The present measurements of the total cross sections of the three osmium isotopes are intended to better define the OMP applicable to the mass region near $A\sim190$ where relatively little is known about the effects of deformation on the OMP.

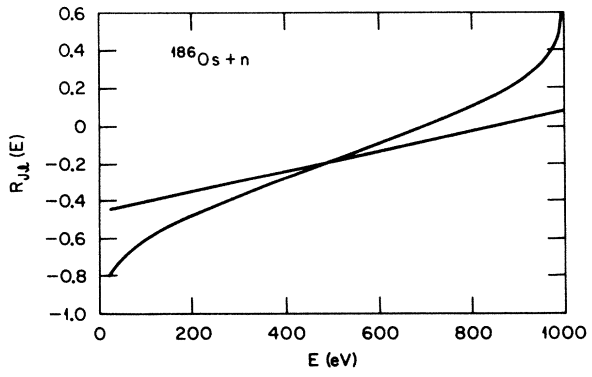

FIG. 4. The external R function (S-shaped curve) and $\tilde{R}$ (linear curve) for ^{186}Os + n.

For an OMP the average scattering matrix (a function in this case) can be written in terms of a smooth complex R function $\bar{R}_{Jl}$,

$$U_{Jl}^{\rm OMP}=e^{2i\phi_l}\frac{1+iP_l\bar{R}_{Jl}}{1-iP_l\bar{R}_{Jl}}\ . \tag{12}$$

The complex R function, $\bar{R}_{Jl}$, has real and imaginary parts which can be identified[17,18,29] with $\tilde{R}$ and $\pi\tilde{s}$. The OMP well depths can be varied until the real and imaginary parts of $\bar{R}_{Jl}$ are equal to the corresponding experimentally determined quantities; i.e.,

$$\mathrm{Re}[\bar{R}_{Jl}(E)]=\tilde{R}_{Jl}(E)\ , \tag{13}$$

$$\mathrm{Im}[\bar{R}_{Jl}(E)]=\pi\tilde{s}_{Jl}\ , \tag{14}$$

where the fitting is done at the midpoint $\bar{E}$ of the range $[E_L,E_u]$. This approach has been extensively pursued at low energies and the results are summarized in Figs. 2 and 3 of Ref. 20. In that work, however, the comparison is with R'_{Jl} rather than with $\tilde{R}_{Jl}$ [see Eq. (8)].

The OMP used in this work consists of a real Woods-Saxon potential plus an imaginary surface term,

$$V^J(r)=-V_0^J f(r)+i4a_D W_D^J\frac{dg(r)}{dr}\ , \tag{15}$$

where

$$f(r)=\{1+\exp[(r-R_0)/a_0]\}^{-1}\ ,$$

$$g(r)=\{1+\exp[(r-R_D)/a_D]\}^{-1}\ ,$$

$$R_0=r_0A^{1/3}\ \text{and}\ R_D=r_DA^{1/3}\ .$$

Since the model consists of six parameters (for each J) and only two experimental quantities are available for fitting, we fixed all geometric parameters at the values given in Table VII. The experimentally observed pairs $(\tilde{R}_{Jl},\tilde{s}_{Jl})$ were then reproduced by varying V_{0l}^{J} and W_{Dl}^{J}. The results of this analysis for ^{186}Os + n are shown in Fig. 5 and the results for all three isotopes in Table VIII. A single OMP describes the $\tilde{R}$ and $\tilde{s}$ for the two even isotopes. The odd mass isotope, however, has a spin-dependent imaginary well depth. The OMP for ^{187}Os with $V_0=48$–49 MeV does not bind the $4s$ single particle state; in fact, this state is located in or just above our experimental region so that the imaginary well must be shallow to produce the observed 0^- strength ($S_0=8.0\times10^{-4}$) but very deep to produce sufficient spreading of the $4s$ state to reduce the 1^- strength to the rather small observed value $S_0=3.2\times10^{-4}$.

Since in most applications, the OMP is required to describe a given partial wave cross section without regard to spin, we have combined the two (0^- and 1^-) shape elastic and the compound nuclear cross sections for ^{187}Os to form s-wave shape elastic and compound nuclear cross sections. The OMP well depths which result from fitting the OMP to these cross sections (rather than to $\tilde{R}$ and $\tilde{s}$) are $V_0=48\pm2$ MeV and $W_D=9\pm1$ MeV. These results are shown in Fig. 6. These effective well depths are essentially the same as for ^{186}Os and ^{188}Os (Table VIII).

The OMP in Table VIII also agrees well with three studies[30–32] of the global mass systematics of the OMP. The deep imaginary well spreads the barely bound $4s_{1/2}$ single-particle state sufficiently to account for the observed distribution of s-wave strength over many levels. This is consistent with the results[33] from (d,p) measurements which find that the single-particle s-wave strength is distributed over a large number of states up to ~1 MeV. This spreading of the single-particle strength can be interpreted as being due to particle-core collective states. Cao *et al.*[34] used a coupled-channel calculation to include such deformation effects on the ^{187}Os cross sections and found a somewhat shallower real well ($V_0\sim46$ MeV for $r_0=1.22$ fm) and an appreciably shallower imaginary well (~4.5 MeV for $r_D=1.26$ fm), thus supporting the idea that the deep imaginary well found in this work and by Hershberger *et al.*[14] is due to deformation effects. Assuming that the product $V_0r_0^2$ is invariant, Cao's value for V_0 is equivalent to ours.

A final consideration which makes clear that the spherical OMP found in this work is local to the osmium mass region is the fact that a real well depth of 50 MeV binds the $4s_{1/2}$ state by only <0.5 MeV. This agrees well with the position of the upper component of the peak in the s-wave strength function near mass 190. However, this OMP cannot account for the lower component near mass

TABLE VII. Optical model potential geometry (all values in fm).

r_0	1.21
a_0	0.66
r_D	1.21
a_D	0.48

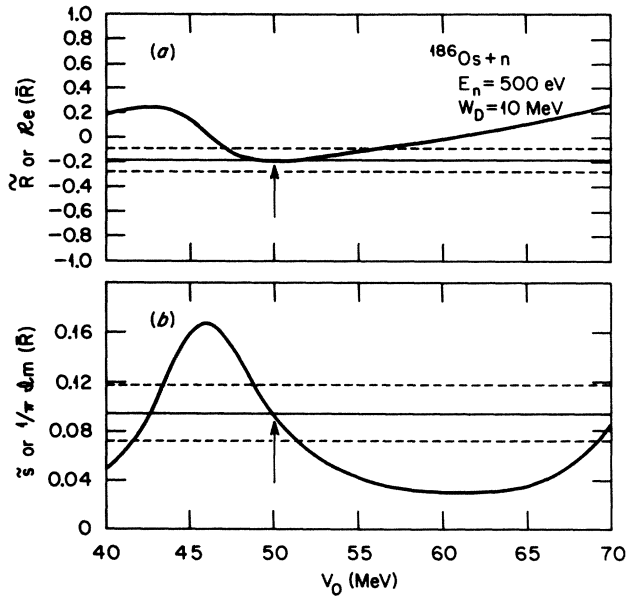

FIG. 5. (a) The real and (b) imaginary (divided by π) parts of the R function calculated using the OMP parameters in Table VIII vs V_0 for a neutron energy of 500 eV. The horizontal solid lines give the observed values of $\tilde{R}$ and $\tilde{s}$ with associated uncertainty estimates as dashed lines. The arrow indicates the value of V_0 (50 MeV) which best describes both $\tilde{R}$ and $\tilde{s}$.

160. A deformed OMP calculation[20] with $V_0=43.5$ MeV, $W_D=5.4$ MeV, and $r_0=1.27$ fm accounts for both peaks (see Fig. 2 in Ref. 20).

VI. THE Re/Os CHRONOMETER

The $^{187}\text{Re}\rightarrow{}^{187}\text{Os}+\beta$ decay with its long half-life (4.2×10^{10} yr) has long[4] been recognized as a potential chronometer for r-process stellar nucleosynthesis. Since ^{187}Os is shielded from production by the r process, the observed abundance of ^{187}Os is presumed to be the sum of that due to the s process and that due to the decay of ^{187}Re. The s-process abundance $N_s(^{187}\text{Os})$ can be calculated using the near constancy of the s-process current (abundance$\times$Maxwellian averaged capture cross section) in the osmium mass region,

$$N_s\langle\sigma_\gamma^*\rangle(187)=N_s\langle\sigma_\gamma^*\rangle(186)\ . \tag{16}$$

Since ^{186}Os is presumably made only by the s process,

TABLE VIII. Best-fit optical model well depths. The OMP and experimental results are compared at incident neutron energy $E_n=500$ eV for ^{186}Os and ^{188}Os and at 70 eV for ^{187}Os.

A	J	V_0 (MeV)	W_D (MeV)
186	$\frac{1}{2}^+$	50(2)[b]	10(2)
187[a]	0^-	48(1)	4(1)
187[a]	1^-	49(3)	15(2)
188	$\frac{1}{2}^+$	48(1)	11(2)

[a]The s-wave cross sections for ^{187}Os are well described by an OMP with $V_0=48\pm2$ MeV and $W_D=9\pm1$ MeV.
[b]In this notation $50(2)\equiv50\pm2$.

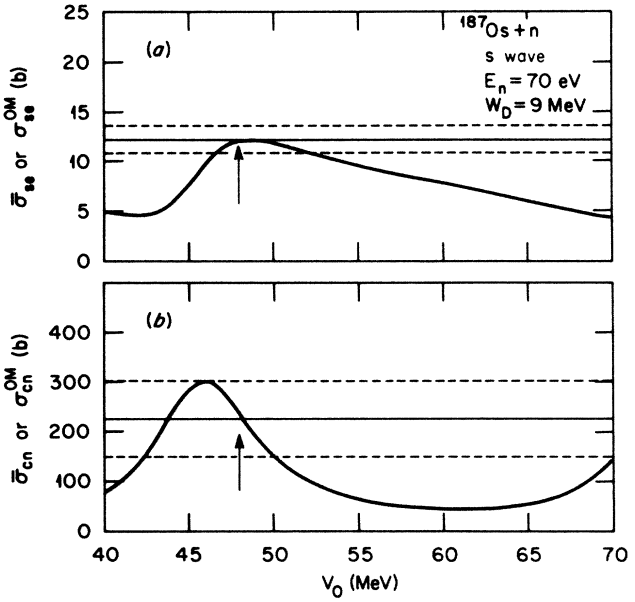

FIG. 6. (a) The shape elastic and (b) compound nucleus cross sections calculated for s-wave neutrons on ^{187}Os vs V_0 for $W_D=9$ MeV. The solid curves give the measured values (obtained by averaging the measured scattering matrix for each spin and then combining the resulting cross sections) and the dashed curves the uncertainty estimates. The arrows indicate the value of V_0 (48 MeV) which best describes the $l=0$ shape elastic and compound nucleus cross section.

$N_s(^{186}\text{Os})$ can be taken as the observed abundance of ^{186}Os. The Maxwellian capture cross sections $\langle\sigma_0^*\rangle$ are those appropriate for the stellar site of the s process ($kT=30$ keV) and can be written in terms of the laboratory cross sections as

$$\langle\sigma_\gamma^*\rangle = f\langle\sigma_\gamma\rangle \ , \tag{17}$$

where f is a stellar enhancement factor. Since the first excited state of ^{186}Os is located at 137 keV, well above stellar thermal excitation energies ($kT=30$ keV), the enhancement factor for ^{186}Os is essentially unity. The first excited state of ^{187}Os, however, is only 10 keV above the ground state and is heavily populated at stellar temperatures. Hence, $\langle\sigma_\gamma^*\rangle(^{187}\text{Os})$ includes the effect of capture by the first excited state as well as the ground state.

Using preliminary results from the present work, Hershberger *et al.*[14] found that a spherical OMP with essentially the same geometry as in Table VII and with $V_0=47.4$ MeV and $W_D=9.6$ MeV gave a good description of the neutron total cross section of the ^{187}Os, as well as the capture and 60-keV inelastic scattering cross sections of ^{187}Os. Thus, the spherical OMP with $V_0\sim 48$ MeV and $W_D=9$ MeV seems adequate for calculations of the ^{187}Os ground-state capture cross section. When this OMP is used, the capture cross section of the first excited state of ^{187}Os is larger than that of the ground state and the stellar enhancement factor for ^{187}Os is $f(187)=1.23\pm0.01$, where the uncertainty includes only the uncertainty estimates given for V_0 and W_D in Table VII. Hershberger *et al.*[14] reported an uncertainty estimate of ±0.03 for $f(187)$ which includes uncertainties associated with calculating the gamma-ray transmission factors as well as those associated with the optical model parameters. Thus, the stellar-enhanced cross-section ratio $\langle\sigma_\gamma^*(^{186}\text{Os})\rangle/\langle\sigma_\gamma^*(^{187}\text{Os})\rangle$ is $f^*=0.81$ times that measured in the laboratory. This result is in good agreement with earlier estimates, $0.8\leq f^*\leq 1.2$, by Holmes *et al.*[35] and Woosley and Fowler[13] based on global Hauser-Feshbach calculations. Detailed discussions of the analysis of the Re/Os chronometer are given in Refs. 4, 36, and 37. Briefly, assuming that the rate of r-process nucleosynthesis decreases exponentially, adopting the measured cross-section ratio $\langle\sigma_\gamma(^{186}\text{Os})\rangle/\langle\sigma_\gamma(^{187}\text{Os})\rangle = 0.4787\pm0.022$ from Ref. 23, and taking the isotopic and elemental abundances from Ref. 38 results in an Re/Os chronometer yield of $\Delta=(11\pm2.5)\times10^9$ yr for the duration of r-process nucleosynthesis. The uncertainty of ±0.03 in the value of f^* accounts for about $\pm0.5\times10^9$ yr in the uncertainty estimate for Δ. The value $(11\pm2.5)\times10^9$ yr is in excellent agreement with the result, $\Delta=(13\pm4)\times10^9$ yr, from a similar analysis[39] based on the U/Th chronometers. Our results for Δ lead to an estimate of the age of the universe, $A_u=17\times10^9$ yr, with an uncertainty of about $\pm3\times10^9$ yr. This value for A_u is comparable to the Hubble time of $H_0^-=(19.5\pm3)\times10^9$ yr determined by Sandage and Tammann[40] and almost twice as large as the value $H_0^{-1}=(10.3\pm0.4)\times10^9$ yr determined by DeVaucouleurs.[41] If some of the other problems[11] associated with the Re/Os chronometer, such as temperature and pressure effects on the beta decay rate, can be solved, this chronometer may help choose between the two contending estimates of A_u derived from observations of distant galaxies.

VII. CONCLUSIONS

The analysis presented in the preceding section makes clear the need to use a locally defined spherical OMP or a deformed OMP for calculations of cross sections in this mass region. Of special concern is the need in astrophysics to calculate the capture cross section for the first excited state of ^{187}Os. This state is similar to the ground state in that both are built on vibrational states which distribute the s-wave strength over many states. Hence, nuclear deformation effects are probably important and a coupled-channel calculation may be needed for reliable estimates of the excited state capture cross section. Based on our spherical OMP, the effect of capture from the first excited state in ^{187}Os at stellar temperatures is to decrease the cross-section ratio $\langle\sigma_\gamma(^{186}\text{Os})\rangle/\langle\sigma_\gamma(^{187}\text{Os})\rangle$ by 20%. With this result, the age of the universe derived from the Re/Os chronometer is $(17\pm3)\times10^9$ yr.

ACKNOWLEDGMENTS

We are very appreciative of the support and encouragement given by Professor W. A. Fowler. Dr. R. L. Macklin and M. T. McEllistrem have contributed significantly to this work with their interest and lively discussions. We also acknowledge the careful work on the part of the

ORELA operators. This research was sponsored by the Division of Nuclear Sciences, U.S. Department of Energy, under Contract No. DE-AC02-76ER02696 with Denison University, Contract No. DE-AS05-80ER10710 with Middle Tennessee State University, and Contract No. DE-AC05-840R21400 with Martin Marietta Energy Systems, Inc.

[1]R. A. Alpher and R. C. Hermann, Rev. Mod. Phys. **22**, 153 (1950).
[2]E. M. Burbridge, G. R. Burbridge, W. A. Fowler, and F. Hoyle, Rev. Mod. Phys. **29**, 547 (1957).
[3]W. A. Fowler and F. Hoyle, Ann. Phys. (N.Y.) **10**, 280 (1960).
[4]D. D. Clayton, Astrophys. J. **139**, 637 (1964).
[5]D. D. Clayton, Nature (London) **224**, 56 (1969).
[6]F. Perrone, Ph.D. thesis, Rice University, 1979 (unpublished).
[7]M. Arnould, Astron. Astrophys. **21**, 401 (1972).
[8]R. J. Talbot, Astrophys. Space Sci. **20**, 247 (1973).
[9]M. Arnould, Astron. Astrophys. **31**, 371 (1974).
[10]J. Conrad and H. D. Zeh, Z. Naturforsh. **33a**, 887 (1978).
[11]K. Tokoi, K. Takahashi, and M. Arnould, Astron. Astrophys. **117**, 65 (1983).
[12]M. Arnould, K. Takahashi, and K. Yokoi, Astron. Astrophys. **137**, 51 (1984).
[13]S. E. Woosley and W. A. Fowler, Astrophys. J. **233**, 411 (1979).
[14]R. L. Hershberger, R. L. Macklin, M. Balakrishnan, N. W. Hill, and M. T. McEllistrem, Phys. Rev. C **28**, 2249 (1983).
[15]R. R. Winters, in *Neutron-Nucleus Collisions: A Probe of Nuclear Structure* (Burr Oak State Park, Ohio, 1984), edited by J. Rapaport, R. W. Finlay, S. M. Grimes and F. S. Dietrich (AIP, New York, 1984) (AIP Conf. Proc. No. 124).
[16]D. C. Larson, C. H. Johnson, J. A. Harvey, and N. W. Hill, Oak Ridge National Laboratory Report No. ORNL/TM-5612, Oak Ridge, Tennessee, 1976 (unpublished); D. C. Larson, N. M. Larson, and J. A. Harvey, Oak Ridge National Laboratory Report No. ORNL/TM-8880, Oak Ridge, Tennessee, 1984 (unpublished).
[17]C. H. Johnson and R. R. Winters, Phys. Rev. C **21**, 2190 (1980); **27**, 416 (1983).
[18]C. H. Johnson, N. M. Larson, C. Mahaux, and R. R. Winters, Phys. Rev. C **2**, 1913 (1983).
[19]C. H. Johnson, C. Mahaux, and R. R. Winters, Phys. Rev. C **32** (1985).
[20]S. F. Mughabghab, *Neutron Cross Sections* (Academic, New York, 1984), Vol. 1, Pt. B.
[21]N. M. Larson, Oak Ridge National Laboratory Report No. ORNL/TM-9179, 1984 (unpublished).
[22]G. F. Auchampaugh, Los Alamos Scientific Laboratory Report No. LA-5473-MS, 1974 (unpublished).
[23]R. R. Winters and R. L. Macklin, Phys. Rev. C **25**, 208 (1982).
[24]J. Browne, private communication.
[25]A. Stolovy, A. I. Namenson, and B. L. Berman, Phys. Rev. C **14**, 965 (1976).
[26]R. Sedlmayr, M. Sedlmayr, and W. Greiner, Nucl. Phys. **A232**, 465 (1974).
[27]F. W. K. Firk, J. E. Lynn, and M. C. Moxon, Proc. Phys. Soc. (London) **82**, 477 (1963).
[28]B. Buck and F. G. Perey, Phys. Rev. Lett. **8**, 444 (1962).
[29]A. M. Lane and R. G. Thomas, Rev. Mod. Phys. **30**, 257 (1958).
[30]C. M. Perey and F. G. Perey, At. Data Nucl. Data Tables **17**, 1 (1976).
[31]B. Holmqvist, Ark. Fys. **38**, 403 (1968).
[32]F. D. Becchetti and G. W. Greenlees, Phys. Rev. **182**, 1190 (1969).
[33]P. Morgen, B. S. Nielsen, J. Onsgaard, and C. Sondergaard, Nucl. Phys. **A204**, 81 (1972).
[34]Z. Cao, R. L. Hershberger, and M. T. McEllistrem, Bull. Am. Phys. Soc. **28**, 997 (1983).
[35]J. A. Holmes, S. E. Woosley, W. A. Fowler, and B. A. Zimmerman, At. Data Nucl. Data Tables **18**, 305 (1976).
[36]J. Browne and B. Berman, Nature (London) **262**, 197 (1976).
[37]R. R. Winters, R. L. Macklin, and J. Halperin, Phys. Rev. C **21**, 563 (1980).
[38]E. Anders and M. Ebihara, Geochim. Cosmochim. Acta **46**, 2363 (1982).
[39]F. K. Thielemann, J. Metzinger, and H. V. Klapdor, Z. Phys. A **309**, 301 (1983).
[40]A. Sandage and G. A. Tammann, Astrophys. J. **256**, 339 (1982).
[41]G. DeVaucouleurs, Astrophys. J. **253**, 520 (1982).